Catalysis Science & Technology

Accepted Manuscript

ROYAL SOCIETY OF CHEMISTRY

www.rsc.org/catalysis

The enhancement of the catalytic performance of CrO_x/Al_2O_3 catalysts for ethylbenzene dehydrogenation through tailored coke deposition

Sara Gomez [a], Liam McMillan [a], James McGregor [a,b*], J. Axel Zeitler [a], Nabil Al-Yassir [c], Sulaiman Al-Khattaf [c], Lynn F. Gladden [a]

[a] University of Cambridge, Department of Chemical Engineering and Biotechnology, Cambridge CB2 3RA, UK

[b] present address: University of Sheffield, Department of Chemical and Biological Engineering, Sheffield S1 3JD, UK

[c] King Fahd University of Petroleum & Minerals, Dhahran 31261, Saudi Arabia

*e-mail: james.mcgregor@sheffield.ac.uk

Abstract

In previous work we have shown that ethylbenzene dehydrogenation over CrO_x/Al_2O_3 catalysts proceeds sequentially *via* cracking and then dehydrogenation reactions. The present work reports how tailored coke deposition on the catalyst surface can suppress undesired reactions such as cracking to benzene and coke during ethylbenzene dehydrogenation. Additionally, this approach also provides insights into the precursor molecules involved in the formation of carbonaceous deposits, hence providing further understanding of coke formation. Pre-coked catalysts were prepared by adsorbing the products of the ethylbenzene reaction (*i.e*, benzene, toluene, styrene, ethylene) as single components, in a flowing system at 600 °C over the fresh catalyst. The resulting pre-coked catalysts were then evaluated in the ethylbenzene dehydrogenation reaction and their performance compared with that of the catalyst without exposure to pre-treatment. Characterisation of pre-coked catalysts by elemental analysis, temperature-programmed oxidation (TPO), temperature-programmed desorption (TPD), Raman spectroscopy and diffuse reflectance infrared Fourier transform spectroscopy (DRIFTS) indicated that ethylene is the main coke precursor during ethylbenzene dehydrogenation and that ethylene-derived coke is associated with a reduction in selectivity to styrene as compared to the fresh catalyst. Coke deposited after pre-coking with aromatic molecules, and in particular with benzene, was beneficial for dehydrogenation activity, as shown by the increase in styrene selectivity relative to the fresh catalyst. This enhancement of dehydrogenation activity was correlated with deactivation of acid sites and the reduction of chromium from Cr(VI) to Cr(III) (active species for dehydrogenation) as a result of the pre-coking procedure.

Keywords: alumina-supported chromia; ethylbenzene dehydrogenation; styrene; coke deposition; pre-coking

1. Introduction

A large number of studies on the influence of carbonaceous deposits on the catalytic activity and selectivity of zeolites [1,2] and metal-oxide catalysts [3,4] are reported in the literature. Most of these investigations refer to the detrimental effect of coke deposition on the catalytic performance by blocking pores or by poisoning the active sites. However, increasingly there is discussion around the idea that certain coke structures can play a beneficial role, and improve selectivity to the desired product [5–8]. Additionally, coke deposits have long been postulated to promote catalytic reactions including hydrogenation through facilitating hydrogen transfer, and methanol-to hydrocarbon conversion through the hydrocarbon pool mechanism [9,10]. Industrially, there is considerable interest that exists in developing methods to enhance the selectivity of products by surface modification of zeolite catalysts. Such methods include pre-treatments that typically imply the inactivation of external active sites [11]. The most effective ways to deactivate non-selective acid sites in zeolites include chemical vapour/liquid deposition of organosilicon compounds [12,13], pre-coking treatment [14,15], selective deactivation of acid sites with basic molecules [16] or impregnation with metals such as cerium [17].

Pre-coking or tailored carbon deposition refers to the controlled laydown of carbonaceous deposits to enhance the selectivity of cracking catalysts and zeolites in hydrocarbon processing. This approach has been used in the past [18] and it enables: i) identification of the molecular species responsible for the generation of the precursors of coke; and ii) enhancement of catalytic performance through poisoning of acid sites, pore blocking or deposition of active coke [19]. Reactions involved in hydrocarbon processing such as alkylation, hydrogenation and isomerisation can be notably improved through tailored pre-coking. For instance, Mandal *et al*. reported that a level of 0.2-0.3% of coke on a regenerated FCC catalyst maximised the fraction of medium distillates and limited over-cracking [20]. Elsewhere, Lee *et al*. [21] showed that *p*-xylene did not react over fresh FCC catalyst at 200 ºC but alkylation occurred if the catalyst had been pre-coked with isopropanol at 500 ºC. A further example where pre-coking has been successfully applied is the selective toluene disproportionation process (MSTDP^{TM}), where the catalyst is pre-coked with aromatic feedstocks at elevated

temperature during the initial stages of the treatment [22,23]. In the work of Haag and co-workers [24,25], pre-coking of HZSM-5 with an aromatic feedstock led to a coke content exceeding ~ 2 wt.% which was sufficient to increase the selectivity to *p*-xylenes from toluene disproportionation. Despite the advantages offered by tailored carbon deposition, there are also examples of ineffective pre-coking in the literature. Laforge *et al*., studied the effect of pre-coking through pre-adsorption of *n*-heptane over MCM-22 for *m*-xylene isomerization [26]. It was concluded that this pre-treatment was not able to selectively deactivate the external acid sites of the zeolite. In addition, pre-coking can cause pore narrowing, hence introducing diffusion limitations which can diminish catalytic performance [27].

The present work focuses on the surface modification of CrO_x/Al_2O_3 by pre-coking the catalyst through adsorbing, in separate experiments, the products of the ethylbenzene dehydrogenation reaction: benzene, toluene, styrene and ethylene. Characterisation of the catalyst surface after pre-coking, but before exposure to the dehydrogenation reaction, and then again post-reaction, enables us to identify the dominant precursor molecules in coke formation during ethylbenzene dehydrogenation and hence how pre-coking might be exploited to suppress undesired reactions such as cracking to benzene and coke during the dehydrogenation reaction. Characterisation of pre-coked catalysts by elemental analysis, temperature-programmed oxidation (TPO), temperature-programmed desorption (TPD), terahertz-time-domain spectroscopy (THz-TDS), Raman spectroscopy and diffuse reflectance infrared Fourier transform spectroscopy (DRIFTS) provides information on the coke structures which improve dehydrogenation activity and the precursor molecules which are responsible for carbon deposition. X-ray photoelectron spectroscopy (XPS) was used to determine the oxidation sates of chromium.

In summary, the aims of this work are to identify: i) if the pre-coking approach can be used to determine the main precursor molecule of coke in ethylbenzene dehydrogenation; and ii) whether or not a pre-coking treatment can suppress undesired reactions, such as cracking to benzene and coke, leading to an enhanced selectivity to dehydrogenation.

2. Experimental

2.1. Catalyst synthesis

An alumina-supported chromia catalyst was prepared by wet impregnation using $Cr(NO_3)_3 \cdot 9\ H_2O$ (Sigma-Aldrich, 99%); the alumina support used was γ-Al_2O_3 (Condea Chemie GmbH, Hamburg, Germany, BET surface area = 216 $m^2\ g^{-1}$). Approximately 15.98 g of $Cr(NO_3)_3 \cdot 9\ H_2O$ and 20 g of γ-Al_2O_3 were added to 300 ml of water. The catalyst precursor was then mixed for 3 h at room temperature to ensure a homogeneous distribution of chromia on the support. The solution was then vacuum filtered and the filtrate was washed with water several times. The as-prepared solid was dried in air at 120 ºC overnight and calcined for 24 h at 600 ºC, also in air. The colour of the catalyst changed from green to yellow after calcination. The chromium loading was 0.8 wt.% which is significantly below monolayer coverage, ~ 12 wt.% [28]. It has been found that below monolayer coverage the predominant surface chromium species are expected to be polymeric and monomeric Cr(VI) [29]. Characterisation of the fresh catalyst by Raman spectroscopy showed bands in the 882-890 cm^{-1} range corresponding to monochromate and polychromate species [30].

2.2. Pre-coking and catalytic activity measurements

Carbonaceous deposits derived from pre-coking with different precursor molecules were formed by pre-adsorbing separately the products of the reaction (benzene, toluene, styrene and ethylene) at 600 °C over CrO_x/Al_2O_3. Pre-coking of CrO_x/Al_2O_3 was carried out using a fixed-bed reactor (inner diameter: 14 mm; total length: 40.2 cm) connected to an on-line GC (Agilent 6890N Series, column Agilent HP-5) equipped with an FID detector and an Agilent HP-5 column. 1 g of CrO_x/Al_2O_3 (particle size, D50: 100 μm; height of bed: 12 mm) was loaded into the reactor and was pretreated under 40 ml/min of helium at 600 °C for 30 min. Adsorbates (benzene, toluene and styrene) were introduced in a saturated He flow *via* a bubbler heated at 70 ºC; the accuracy of the outlet composition was 5%. The flow was adjusted to feed the same number of carbon molecules of precursor into the reactor for a period of 360 min (3.2×10^{23} carbon molecules) and to ensure a total volumetric flow rate of 45 ml/min of helium and ethylbenzene. In the case of ethylene pre-coking, 16.5 ml/min of ethylene (99.99%, Air

Liquide) were mixed with 28.5 ml/min of helium and preheated at 70 ºC, thereby maintaining the overall amount of carbon molecules fed to the reactor for 360 min (3.2×10^{23} carbon molecules).

Ethylbenzene dehydrogenation over CrO_x/Al_2O_3 and pre-coked catalysts was performed in the same reactor set-up as used for pre-coking. Approximately 1 g of CrO_x/Al_2O_3 catalyst was pretreated under helium (1 barg, 40 ml/min) at 600 °C for 30 min. After this period, 40 ml/min of helium were flowed through a saturator filled with ethylbenzene at 70 ºC. The reactor was fed with 45 ml/min of a mixture of helium and ethylbenzene maintaining a helium/ethylbenzene ratio of 7.75 at atmospheric pressure. Gas chromatography measurements were taken every 20 min during a total reaction time of 360 min. Conversion and selectivity to benzene, toluene, styrene and coke were determined according to Equations (1) and (2) and averaged over the steady-state regime. It should be noted that conversion is calculated considering conversion to all products including coke. Selectivity to coke was calculated by applying a carbon mass balance as shown in Equation (3). After 6 h the catalyst was cooled down under 40 ml/min helium and removed for subsequent characterisation.

$$conversion = \frac{n_{ethylbenzene,in} - n_{ethylbnezene,out}}{n_{ethylbenzene,in}} \cdot 100 \quad (1)$$

$$selectivity_i = \frac{n_{i,out}}{n_{benzene} + n_{toluene} + n_{styrene} + n_{methane} + n_{ethylene} + n_{coke}} \cdot 100 \quad (2)$$

where i = benzene, toluene, styrene and coke

$$n_{coke} = n(C_{ethylbenzene,in}) - n(C_{ethylbenzene,out}) - n(C_{products,out}) \quad (3)$$

2.3. Characterisation techniques

The catalysts were characterised after pre-coking but before exposure to the ethylbenzene dehydrogenation reaction, and then again post-reaction, using a variety of techniques.

Elemental analysis (Microanalytical Department, Department of Chemistry, University of Cambridge) was employed in order to determine the percentages of carbon, hydrogen and nitrogen present. The determination of C/H ratio was conducted *via* combustion of the coked samples in pure oxygen at 950 ºC. The resulting carbon dioxide, water and nitrogen were measured using thermal conductivity detectors. The instrument utilised was an Exeter Analytical CE-440 elemental analyser.

TPO was conducted on the coked catalysts in a Catlab Microreactor Module connected to an online quadrupole mass spectrometer. A gas mixture of composition 5% O_2/He at a total flow rate of 40 ml/min was used. The heating rate was 10 °C/min from 50 ºC to 875 °C. TPD was performed in the same equipment by heating the catalyst from 50 ºC to 900 °C at a rate of 10 °C/min under a helium flow rate of 40 ml/min.

THz-TDS measurements were performed at 293 K on a spectrometer described previously [31,32]. Samples were prepared by mixing 50 mg of coked catalyst with 150 mg of polyethylene (Sigma-Aldrich) which is transparent to THz radiation.

Raman spectroscopy experiments were conducted using a Raman spectrometer employing a 784.41 nm laser excitation (3 mW) at 5 cm^{-1} spectral resolution (Raman Rxn1 Systems, Kaiser Optical Systems Inc. supplied by Clairet Scientific). Samples were placed on a cover glass at room temperature. Exposure time was 2 min and the laser power was set at 50 mW in order to minimise fluorescence/coke combustion effects. Spectra of both the fresh catalyst and empty sample holder were recorded for subsequent background subtractions. The spectra were fitted by using four components (G, D1, D3 and D4) and analysed in terms of positions, relative intensity and full width at half maximum amplitude (FWHM).

DRIFTS spectra were obtained without sample dilution in a Thermo Nicolet NEXUS 670 spectrometer equipped with a diffuse reflectance attachment and MCT detector. The measurements were performed at room temperature by adding 128 scans at a resolution of 4 cm^{-1}. The spectrum of fresh CrO_x/Al_2O_3 was recorded as a background

and subtracted from the spectra of pre-coked catalysts, such that the observed infrared absorptions could be attributed to the coke deposits present on the catalyst surface.

XPS analyses were carried out at the Sheffield Surface Analysis Centre, (SSAC), Sheffield. XPS experiments of coked CrO_x/Al_2O_3 after ethylbenzene dehydrogenation were conducted to analyse the oxidation states of chromium. These experiments were performed on an Axis Ultra DLD (Kratos) with a monochromated Al-K_α X-ray source operated in electrostatic mode. The vacuum during analysis was *ca.* 1×10^{-8} mbar. Spectral analysis was carried out using CasaXPSsoftware (Casa, http://www.casaxps.com, UK); survey and narrow scan C1s and O1s spectra were obtained.

3. Results

3.1. Catalytic activity measurements

As discussed in a previous study [33], the reaction profile of ethylbenzene dehydrogenation over fresh CrO_x/Al_2O_3 at 600 °C shows two well defined periods of activity (Fig. 1): (i) an induction period before 3 h time-on-stream characterised by cracking activity; ii) styrene breakthrough after 3 h time-on-stream where dehydrogenation activity prevails. Cracking products such as benzene and toluene are mainly formed during the first 3 h of reaction time with maximum selectivity values of 23% and 5%. Selectivity to styrene reaches a maximum after 165 min (25%) prior to achieving a steady-state value of 15% with an ethylbenzene conversion of 97%. Selectivity to coke after 6 h time-on-stream is 81%.

3.2. Study of the nature of coke formed by tailored carbon deposition

After pre-coking, but prior to exposure to the ethylbenzene dehydrogenation reaction, the catalysts pre-coked with different molecules were characterised using the methods described in Section 2. Alongside these data, catalytic activity measurements were performed and are reported in Section 3.3. These data are then used: i) to determine which reactant/product is the main precursor molecule of coke in ethylbenzene dehydrogenation and ii) to assess whether a pre-coking method can be used to suppress undesired side reactions such as cracking to benzene or coke.

The results of the characterisation of the pre-coked catalysts before exposure to the ethylbenzene dehydrogenation reaction are now presented.

Elemental analysis. As reported in Table 1, CrO_x/Al_2O_3 pre-coked with aromatic molecules showed the highest carbon contents (11.1, 10.7 and 8.9 wt%, for benzene, styrene and toluene, respectively). In contrast, the coke content deposited on the ethylene pre-coked catalyst is much lower, at 2.7 wt%. This value approaches the sensitivity limit of the equipment, therefore no accurate conclusion can be drawn as to the type of coke structure for the catalyst pre-coked with ethylene. By comparing the data in Table 1 with the listing of classification of coke structures according to their C/H mass ratio and $\%C_{coke}$, as tabulated in Table 2, some inferences as to the nature of the deposited coke can be made. However, it is important to note that the heterogeneous nature of carbonaceous structures makes their identification a complex process. The values of C/H ratio and $\%C_{coke}$ yielded by elemental analysis are average values corresponding to an average coke structure, which may differ significantly from the actual coke structure. Nevertheless, the values of C/H ratio and $\%C_{coke}$ for the catalyst pre-coked with benzene and styrene fall, on average, in the range corresponding to polyaromatic coke compounds with *n* membered-rings. The C/H ratio and $\%C_{coke}$ for the catalyst pre-coked with toluene are 9.9 and 90.8%, values that on average, correspond to alkylaromatic coke compounds. Since elemental analysis provides a quantification of average coke structures, complementary data from other characterisation techniques (*e.g.*, TPO, Raman, DRIFTS, *etc.*) are required in order to gain a greater understanding of the coke structures present.

Temperature-programmed oxidation (TPO). TPO measurements are shown in Fig. 2. The oxidation temperature allows discrimination between coke of different types [34]; in particular, hydrogen-rich coke deposits are oxidised at temperatures lower than 327 °C, while highly condensed or polyaromatic coke is oxidised at higher temperatures of ~ 427 °C. The area of the TPO bands is related to the amount of carbon-containing material present. By comparing the oxidation temperature of each pre-coked sample with that of the fresh catalyst coked at 600 °C after ethylbenzene dehydrogenation (non-pre-coked catalyst), an indication as to the nature of the precursor molecule of coke

(benzene, toluene, styrene or ethylene) can be elucidated. As seen from Fig. 2, the oxidation temperature of the coked CrO_x/Al_2O_3 catalyst after ethylbenzene dehydrogenation is ~ 455 ºC. The temperature at which the maximum intensity of the TPO peak falls for each of the precursor molecules is 495, 491, 483 and 463 ºC for benzene, styrene, toluene, and ethylene, respectively. The oxidation temperatures of the catalysts pre-coked with benzene, toluene and styrene are significantly higher than the oxidation temperature over the non-pre-coked catalyst, which is indicative of the higher polyaromaticity of the coke laid down over the pre-coked catalysts. In contrast, the oxidation temperature of coke deposited from ethylene pre-coking is very close to that of the fresh catalyst after ethylbenzene dehydrogenation. Additionally, we have previously observed that oxidation temperature is a function of coke precursor and does not vary significantly with time-on-stream [33]. This suggests that the chemical nature of coke laid down over the non-pre-coked catalyst is similar to that observed over the catalyst pre-coked with ethylene.

Temperature-programmed desorption (TPD). This technique allows the identification of adsorption sites on the catalyst and provides information on the initial adsorbed species for dehydrogenation over the pre-coked CrO_x/Al_2O_3. The species desorbed were analysed by mass spectrometry and the mass-to-charge ratios monitored were m/z=91 (toluene), m/z=78 (benzene), m/z=104 (styrene), m/z=106 (ethylbenzene) and m/z=28 (ethylene).

The TPD of the catalyst after pre-coking with toluene (Fig. 3a) shows a peak at 165 ºC which is associated with toluene physisorption. The signal for m/z=78, *i.e.* for coke which has undergone decomposition into benzene, shows a main band at 600 ºC with a shoulder at 750 ºC. For the catalyst pre-coked with benzene (Fig. 3b) the TPD profile only shows one band at 800 ºC for m/z=78. The TPD of CrO_x/Al_2O_3 after pre-coking with styrene (Fig. 3c) shows peaks at 210 ºC (both for m/z=104 and m/z=78) due to styrene physisorption and also bands at 600 and 750 ºC for m/z=78. Therefore, there are three adsorption sites (at 600, 750 and 800 ºC) characterised by different adsorption energies where coke is formed. Since the low energy adsorption site (600 ºC) is only present for the alkyaromatic adsorbates (toluene and styrene) it is proposed that it corresponds to a dealkylation site. In contrast, the 750 and 800 ºC bands appear for the catalysts pre-coked with styrene, benzene and toluene, therefore these sites may

correspond to cracking centres with increasing adsorption strength. Finally, the TPD profile of the catalyst after pre-coking with ethylene (Fig. 3d) shows very poor signal-to-noise due to the low amount of coke present. Small peaks observed between 170 and 300 °C are attributed to physisorbed ethylene and the main band at 450 °C is ascribed to CO released due to thermal decomposition of coke.

Raman spectroscopy. The position of the Raman bands and the D1/G and D1/D3 ratios of the pre-coked catalysts after reaction are shown in Table S1. The method of analysis follows that reported previously [33]. Deconvolution of D1, D3 and D4 bands was performed by considering Gaussian-shaped peaks whereas the G band was fitted with a Lorentzian function. Both D1/G and D1/D3 ratios were determined in order to characterise the degree of graphitic order or structural organisation of the coke. At D1/G values greater than 1.1 this parameter is not reliable for the determination of the degree of order of the carbonaceous deposits present [35]. Therefore D1/D3 is a better indicator of the structural order of coke in this work. Fitting was performed by setting the positions of these bands according to the values reported in the literature for carbonaceous materials [36,37] and establishing a boundary of ± 10 cm^{-1}. Values of FWHM were allowed to vary freely. The analysis suggests that coke formed over the catalyst pre-coked with benzene is the most graphitic as it shows the highest D1/D3 ratio (4.0) whereas coke laid down after ethylene pre-coking shows the lowest graphiticity (1.9). For all the pre-coked catalysts, the G band is shifted to values higher than 1580 cm^{-1} which is indicative of a low degree of condensation. The D4 band is more intense for the catalysts pre-coked with toluene and styrene; this feature is associated with sp^2-sp^3 bonds or C–C and C=C stretching vibrations of polyene-like structures [37].

The Raman spectra of the fresh CrO_x/Al_2O_3 catalyst after ethylbenzene dehydrogenation (with no pre-coking)(dotted lines) and the pre-coked catalysts (solid lines) are shown in Fig. 4. The shape of the spectra as well as the position and width of the D1 and G bands allows comparison between the nature of coke derived from precursor molecules and that from ethylbenzene dehydrogenation over the fresh catalyst. The position of the G band for all the pre-coked catalysts is very similar to that of the fresh catalyst after reaction. However, significant differences are observed in the position of the D1 band, especially for the catalysts pre-coked with aromatic molecules (Fig. 4a, b, c). For

instance, the D1 band for the catalyst pre-coked with benzene appears at 1303 cm^{-1} whereas it is located at 1363 cm^{-1} for the fresh catalyst after reaction (Fig. 4b). This is indicative of the more polyaromatic nature of the coke deposited after pre-coking with benzene. Conversely, both the D1 and G bands appear practically at the same Raman shift for the CrO_x/Al_2O_3 pre-coked with ethylene and the fresh catalyst after reaction (Fig. 4d). In addition, their similar band widths and spectral shapes reflect that the structure of coke laid down after reaction over the fresh CrO_x/Al_2O_3 catalyst is similar to that formed after pre-coking with ethylene, in agreement with TPO data.

Diffuse-reflectance infrared Fourier transform spectroscopy (DRIFTS). Fig. 5 shows the DRIFTS difference spectra of the pre-coked catalysts obtained by subtracting the spectrum of the fresh CrO_x/Al_2O_3 catalyst from those of the pre-coked catalysts. The difference spectra of the catalysts pre-coked with aromatic molecules are very similar. The positive absorptions at 1470-1430 cm^{-1} and 1380-1365 cm^{-1} are due to methyl C-H asymmetric and symmetric bending, respectively [38]. The bands at 1580-1560 cm^{-1} are attributed to stretching of aromatic rings. The bands at 958-953 cm^{-1} can be ascribed to aromatic C-H in-plane bending [39]. The absorptions between 850 and 670 cm^{-1} are assigned to C-H out-of-plane bending in an aromatic ring. The location of these bands provides information about the nature of the substitution and allows discrimination between mono-, di- or poly-substitutions [39]. A band located around 816 cm^{-1} is observed as a shoulder of the 958 cm^{-1} band for the catalyst pre-coked with toluene suggesting *para*-substitution of the aromatic rings. This band has a lower intensity for the catalysts pre-coked with benzene and styrene indicating the presence of less substituted polyaromatic coke compounds. The catalyst pre-coked with ethylene shows an intense positive band at 1580 cm^{-1} revealing the presence of aromatic rings. There is also strong absorption at 1470, 1430 and 1370 cm^{-1} associated with methyl C-H asymmetric and symmetric bending. The single absorption located at 833 cm^{-1} reflects *para*-substitution of aromatic rings. The small band at 1730 cm^{-1} is ascribed to carbonyl compounds [38].

Five negative bands are also present for all the pre-coked catalysts: i) a broad band centered at around 1100 cm^{-1} which is due to the contribution of Cr=O groups associated with Cr(VI)-O species (~1000 cm^{-1}) and Al-O stretching vibrations (1200-700 cm^{-1}) [40]; ii) the band at 1650 cm^{-1} associated with uncharged molecular adsorbed

oxygen on Cr(VI)-O sites [41,42]; iii) the weak-moderate absorption centered around 2100 cm^{-1} assigned to chromates or Cr(VI)-O sites [43]; iv) the broad band located at 3520 cm^{-1} indicative of hydroxyl groups on the alumina support [44]; and v) the band at 1650 cm^{-1} corresponding to the bending vibration of H_2O [45]. It is clearly seen that pre-coking causes significant loss of these five functionalities indicating that this treatment blocks the acid sites (as shown by the removal of hydroxyl groups) and reduces the catalyst to Cr(III), as mirrored by the loss of Cr(VI)-O sites. However, coke derived from aromatic molecules (benzene, toluene and styrene) is more effective than coke derived from ethylene at removing these functionalities as shown by the greater negative intensity of OH, Cr(VI)-O and Al-O (Fig. 5 a,b,c).

The DRIFTS spectrum of the fresh catalyst after ethylbenzene dehydrogenation at 600 ºC is shown in Fig. 6. The positive bands at 1580 and 1500 cm^{-1} are associated with aromatic ring stretching. The absorptions at 1470, 1420 and the shoulder at 1370 cm^{-1} correspond to methyl C-H asymmetric and symmetric bending. The small band centred at 1710 cm^{-1} shows the presence of carbonyl compounds [39]. By comparing the coke region (1700-1300 cm^{-1}) of the spectrum shown in Fig. 6 with those of the pre-coked catalysts (Fig. 5), there are clear similarities between the coke deposited on CrO_x/Al_2O_3 during ethylbenzene dehydrogenation and on the catalyst pre-coked with ethylene. The similarity between the DRIFTS spectra of the pre-coked catalyst with ethylene and the fresh catalyst after ethylbenzene dehydrogenation (Fig. 5d and Fig. 6) is due to the presence of similar carbonaceous structures. To confirm that the similarity between the bands shown in Figs 5d and 6 can be unambiguously assigned to the similar nature of the carbon deposited as opposed to the amount of coke deposited, a sample of the catalyst with a much higher level of pre-coking with the ethylene precursor was analysed. The features obtained from DRIFTS analysis was identical to those seen in Figs 5d and 6.

In an attempt to assign chemical structures to the coke deposited after pre-coking, the DRIFTS spectra shown in Fig. 5 were compared with spectra of typical model coke compounds including alkylbenzenes and polyaromatic compounds (NIST Chemistry Web Book; http:/webbook.nist.gov). Fig. 7 shows the infrared spectra of 1-methyl naphthalene (Fig. 7a) and *p*-xylene (Fig. 7b) as two examples. It can be observed that

the catalysts pre-coked with aromatic molecules (Fig. 5a,b,c) exhibit a structure similar to 1-methyl naphthalene (Fig. 7a) as shown by the weak absorptions at 1570, 1450 and 1370 cm^{-1}. In contrast, the spectra of the catalyst pre-coked with ethylene (Fig. 5d) and that of fresh CrO_x/Al_2O_3 after ethylbenzene dehydrogenation (Fig. 6) are consistent with a more discrete, molecular structure similar to that of *p*-xylene (Fig. 7b). While the coke structures are likely to be heterogeneous in nature, this analysis indicates likely differences in the degree of condensation of the coke formed.

3.3. Reaction of Pre-Coked Catalysts and Characterisation of Post-Reaction Materials

In the following section the catalytic performance of the pre-coked catalysts is presented, along with the characterisation of the pre-coked catalysts following exposure to the ethylbenzene dehydrogenation reaction.

3.3.1. Ethylbenzene dehydrogenation over pre-coked catalysts

Ethylbenzene dehydrogenation was performed over the fresh CrO_x/Al_2O_3 (Fig. 1) and the pre-coked catalysts (Fig. 8). As shown in Fig. 1, the selectivities to benzene and toluene are high over the cracking period (0-3 h) for the fresh catalyst. Conversely, for all the pre-coked catalysts (Fig. 8) there is no formation of benzene and toluene as evidenced by the fact that no induction time is observed, which suggests that the pre-coking treatment blocks the acid sites of the alumina support. It is noted that for the catalyst pre-coked with toluene (Fig. 8a) the selectivity to styrene increases monotonically to 42% at 165 min time-on-stream and then decreases, levelling-off at ~24% at 245 min, in a similar manner to the fresh catalyst after ethylbenzene dehydrogenation (Fig. 1). In a previous study [33], it was observed that methane was produced as a co-product of ethylbenzene hydrogenolysis into toluene and from CO methanation during ethylbenzene dehydrogenation. For the catalyst pre-coked with toluene, formation of methane was also observed during ethylbenzene dehydrogenation. Furthermore, water was present in the gas phase due to dehydration of surface hydroxyl groups and further chromium reduction by ethylbenzene [33]. The change in selectivity to

styrene at 165 min (Fig. 8a) may be due to the competition between, on the one hand, ethylbenzene steam reforming and CO methanation and, on the other hand, ethylbenzene dehydrogenation.

The selectivity to styrene for the catalysts pre-coked with aromatic molecules was compared to that of the fresh catalyst. The higher selectivity obtained over the catalysts pre-coked with aromatic molecules was correlated with the deactivation of Cr=O sites associated with Cr(VI)-O species caused by the pre-coking treatment. These results were also confirmed by DRIFTS studies of the pre-coked catalysts (Fig. 5). Table 3 shows the values of conversion and selectivity for the fresh and pre-coked catalysts after ethylbenzene dehydrogenation. The selectivities to styrene and coke for the fresh catalyst were 15.1% and 80.1%, respectively. The comparison of these values with those of the pre-coked catalysts identifies benzene as the best coking agent in terms of improving catalytic performance, with the highest selectivity to styrene (31.0%) and the lowest selectivity to coke (66.7%). Similar values of catalytic activity are observed for the catalyst pre-coked with styrene (29.1 % selectivity to styrene and 69.1% selectivity to coke). In contrast, pre-coking with ethylene gives the lowest selectivity to styrene (11.4%) and the highest selectivity to coke (87.3%). Further investigation was conducted to confirm the process responsible for the improvement in styrene selectivity for the catalyst pre-coked with benzene, *i.e.* whether it results from selective deactivation of acid sites or from a change in chromium oxidation state. The catalyst acidity and the distribution of chromium sites were studied by NH_3-TPD and XPS, respectively. The methods of analysis follow those described previously [33]. Table 4 shows the number and distribution of acid sites, as determined by NH_3-TPD, for fresh CrO_x/Al_2O_3, CrO_x/Al_2O_3 after ethylbenzene dehydrogenation at different times-on-stream and CrO_x/Al_2O_3 pre-coked with benzene. Acid sites were classified according to their desorption temperature into low energy acid sites (<250 °C), medium energy acid sites (250–400 °C) and high energy acid sites (>400 °C) [46]. A higher percentage of low and high energy acid sites are poisoned after benzene pre-coking as compared to medium strength acid sites. The low strength acid sites decreased from 202 to 86 μmol NH_3/g after pre-coking, while the high energy acid sites decreased from 101 to 42 μmol NH_3/g. In contrast, the medium strength acid sites were poisoned to a lesser extent, decreasing from 191 to 115 μmol NH_3/g after pre-coking. Fig. S1 shows the XPS

spectra of the fresh CrO_x/Al_2O_3 and the catalyst pre-coked with benzene. The oxidation states of chromia were analysed by deconvoluting the peaks present between 570 and 600 eV. The Cr(III)/Cr(VI) ratios for the fresh and pre-coked catalyst with benzene are shown in Table 5. For the fresh catalyst, the Cr(III)/Cr(VI) ratio is low (0.3) suggesting that after calcination the main species in the catalyst is Cr(VI) as has been previously reported by other authors [47,48]. However, after pre-coking with benzene, the Cr(III)/Cr(VI) ratio increases to a value of 1.2 which indicates that chromium is partly reduced to Cr(III). Given that dehydrogenation activity was observed for the catalyst pre-coked with benzene from the beginning of the reaction, the lower value of the Cr(III)/Cr(VI) ratio of the pre-coked catalyst with benzene (1.2) as compared to the fresh catalyst after 3 h of ethylbenzene dehydrogenation (2.2) suggests that the extent of chromium reduction is not directly correlated with: i) the observed selectivity to styrene; or ii) the length of the induction time before dehydrogenation occurs. Therefore, while the presence of Cr(III) is required for dehydrogenation, the selective deactivation of acid sites, which inhibits side-reactions, plays a critical role in obtaining high selectivities to styrene.

In order to identify the type of coke laid down during pre-coking which is beneficial for dehydrogenation activity, the selectivity to styrene over the pre-coked catalysts was correlated with the chemical nature of coke deposited after pre-coking. Fig. 9 shows the selectivity to styrene after ethylbenzene dehydrogenation over the pre-coked catalysts *versus* four characteristics of the deposited coke; namely: the C/H ratio, oxidation temperature, THz absorption coefficient at 1 THz and percentage of reduction of the OH band. Fig. 9a – c show that higher selectivities to styrene are obtained when highly ordered coke deposits are laid down during pre-coking. Furthermore, selectivity to dehydrogenation increases with decreasing concentration of hydroxyl groups (Fig. 9d). These data suggest that highly-ordered carbonaceous deposits are more effective at deactivating hydroxyl groups and hence increase dehydrogenation selectivity.

3.3.2 *Characterisation of pre-coked catalysts after reaction*

Elemental analysis. The data shown in Tables 1 and 7 allow comparison between the carbon-containing compounds on the pre-coked catalyst before (Table 1) and after (Table 6) the dehydrogenation reaction. As shown in Table 6 the carbon percentage

after ethylbenzene dehydrogenation over benzene pre-coked CrO_x/Al_2O_3 (13.5%) only increases slightly relative to the catalysts pre-coked with benzene (11.1%). This demonstrates that more than 97% of coke arises from the pre-coking treatment, suggesting that benzene adsorbs strongly over the acid sites or causes pore blockage, hence limiting coking during ethylbenzene dehydrogenation. Also, the nature of coke does not change substantially given the very similar C/H values of the pre-coked catalyst with benzene (13.9) and the catalyst after reaction (15.0). In contrast, for the catalysts pre-coked with toluene and styrene, the percentages of carbon after ethylbenzene dehydrogenation approximately doubled as compared to the pre-coked catalyst (from 8.9 to 15.4 for toluene; and 10.7 to 21.4, for styrene), indicating that these two precursor molecules have a lower ability to reduce coke deposition. The percentage of carbon deposited over the catalyst pre-coked with ethylene after reaction is substantially higher (14.9%) as compared to the pre-coked catalyst (2.7%). These data show that pre-coking with benzene is most effective at reducing coke formation during ethylbenzene dehydrogenation, whilst ethylene is the least effective pre-coking agent in this regard.

Temperature-programmed oxidation (TPO). The TPO profiles measured over the pre-coked catalysts after ethylbenzene dehydrogenation (Fig. 10) were compared to those of the pre-coked catalysts (Fig. 2). The peak intensities observed for the pre-coked CrO_x/Al_2O_3 are lower than those of the reacted catalysts, consistent with the increase in the carbon percentage after reaction, as seen in the elemental analysis data (Table 6). In addition, there is a significant shift in the oxidation temperature between the styrene pre-coked CrO_x/Al_2O_3 (483 °C) and the reacted catalyst after pre-coking with styrene (532 °C), reflecting a change in coke structure from more disordered to more ordered carbon deposits. A smaller change in the oxidation temperature is observed between the pre-coked and reacted catalysts for the toluene and benzene precursors: from 483 to 498 ºC for the pre-coked catalyst with toluene and after reaction, respectively; and from 495 to 505 ºC in the case of benzene. In the case of the catalyst pre-coked with ethylene there is an increase in the oxidation temperature from 450 ºC after pre-coking to 550 ºC after reaction.

THz-Time Domain Spectroscopy (THz-TDS). THz-TDS provides a qualitative assessment of the degree of graphitic order of coke formed over the pre-coked and reacted catalysts. The THz spectra of the pre-coked and reacted catalysts are shown in Fig. 11. In general, the values of the THz absorption coefficient are relatively low, indicating that the coke structures are disordered in nature. Furthermore, THz absorption is generally lower for the pre-coked catalysts (Fig. 11b, c, d, h) than for the reacted CrO_x/Al_2O_3 (Fig. 11e, f, g, i) which demonstrates the gradual development of the carbonaceous network after reaction. This increase in the absorption coefficient is much less significant for CrO_x/Al_2O_3 pre-coked with benzene (Fig. 11d) and the same catalyst after reaction (Fig. 11e), indicating that after ethylbenzene dehydrogenation over the catalyst pre-coked with benzene the degree of order remains practically unaltered, in agreement with TPO data.

Raman spectroscopy. The maximum value of the D1/D3 ratio (Table 7) is obtained for the pre-coked catalyst with ethylene after ethylbenzene dehydrogenation (4.9) which indicates that the coke present on this sample has the highest degree of graphiticity. The catalysts pre-coked with styrene and toluene after reaction exhibit the lowest values of D1/D3 ratios (2.8 and 2.3, respectively) which reflects the presence of coke with lower degree of structural organisation. These results confirm the trends indicated by THz-TDS (Fig. 11) and TPO (Fig. 10).

4. Discussion

4.1 Use of pre-coking to identify the main precursor molecule of carbon deposits

In this investigation, tailored carbon deposition was employed to elucidate the precursor molecule associated with coke deposition during ethylbenzene dehydrogenation. The identification of the precursor molecule was performed through the comparison between the nature of coke deposited over the fresh catalyst during ethylbenzene dehydrogenation and over the pre-coked catalysts. The different characterisation techniques provided insights into this. For instance, the TPO profile of the catalyst pre-coked with ethylene showed a similar oxidation temperature (463 ºC) to the fresh catalyst after ethylbenzene dehydrogenation (455 ºC) (Fig. 2). In contrast, the catalysts

pre-coked with aromatic molecules exhibited higher oxidation temperatures than the fresh CrO_x/Al_2O_3 after ethylbenzene dehydrogenation, consistent with their higher polyaromaticity (Fig. 2). The clear resemblance between the Raman spectra of the catalyst pre-coked with ethylene and the fresh catalyst after reaction further confirms the similarity between coke formed during ethylbenzene dehydrogenation and ethylene-derived coke (Fig. 4d). The analysis of the nature of coke by DRIFTS spectroscopy yields the same conclusion. Similar bands were observed in the 1700-1300 cm^{-1} region for the catalyst pre-coked with ethylene and the fresh catalyst after reaction (Fig. 5d and Fig. 6). Coke analysis by DRIFTS also showed that ethylene-derived coke is formed by molecular and discrete carbonaceous structures similar, *e.g.*, to *p*-xylene (Fig. 5d and Fig. 7b) suggesting that a significant quantity of the coke deposits comprise *para*-substituted aromatics. The catalysts pre-coked with aromatic molecules exhibited structures similar to naphthenic compounds such as 1-methyl naphthalene (Fig. 5a, b, c and Fig. 7b), significantly different from those on the fresh catalyst after ethylbenzene dehydrogenation (Fig. 6). The data presented provide strong evidence that ethylene is the main coke precursor during ethylbenzene dehydrogenation and that coke derived from ethylene is associated with a reduction in selectivity to styrene during ethylbenzene dehydrogenation compared to the performance of the fresh catalyst.

Based on the characterisation of the ethylene-derived coke structures it is also possible to propose a mechanism for coke formation on the catalyst surface. The formation of alkylated benzene species such as *p*-xylene could proceed through a three-step mechanism as previously described [49]: i) ethylene trimerization into hexene; ii) Diels-Alder reaction between 2,4-hexadiene and ethylene to yield 3,6-dimethylcyclohexene; and iii) dehydrogenation of 3,6-dimethylcyclohexene to form *p*-xylene. Alternatively, chromium oxide-silica-alumina catalysts are known to catalyse the oligomerization of ethylene [50], which can be followed by the transfer dehydrogenation / Diels-Alder reactions to produce *p*-xylene [51,52]. These mechanisms provide potential routes from the ethylene precursor to the coke structures identified on both the ethylene pre-coked catalyst and the non-pre-coked catalyst after reaction. In contrast, for the catalysts pre-coked with aromatic molecules the coke deposits have been observed to differ from those formed on the fresh catalyst after ethylbenzene dehydrogenation and instead show similar structures to naphthenic compounds. These

species may form from either the direct condensation of benzene rings of a hydrogen-C_2H_2 addition pathway [53].

4.2 The effect of pre-coking on suppressing undesired reactions

The catalytic evaluation of the pre-coked catalysts for the dehydrogenation of ethylbenzene (Fig. 8) showed that pre-coking with aromatic molecules led to the inhibition of side-reactions catalysed by acid sites: *i.e.* cracking to benzene and coke, hydrogenolysis of ethylbenzene into toluene and dealkylation of ethylbenzene and toluene. As seen from the reactor data, pre-coking with benzene was the most effective in enhancing selectivity to benzene, but this pre-coking treatment was only slightly better than when pre-coking with styrene. The data shown in Fig. 9, show that when pre-coking increases selectivity to styrene, the effect of pre-coking is to produce coke with relatively higher C/H ratio, and which is more structurally ordered. Furthermore, in these cases a greater reduction in hydroxyl density on the catalyst surface is observed. Whilst there is little difference between the performance of styrene and benzene as pre-coking agents, the data shown in Fig. 9 b,c might suggest that benzene produces a more ordered, thermally stable coke structure than styrene and that this has a greater influence on selectivity than the absolute reduction in the number of hydroxyl groups present.

5. Conclusions

This investigation has demonstrated that pre-coking is a useful strategy to identify the main precursor molecule of coke in ethylbenzene dehydrogenation over CrO_x/Al_2O_3 catalysts. The characterisation of pre-coked catalysts by elemental analysis, TPO, Raman spectroscopy and DRIFTS showed that ethylene is the main coke precursor in ethylbenzene dehydrogenation over CrO_x/Al_2O_3 catalysts and that the nature of coke is *para*-substituted aromatic species. Furthermore, the pre-coking treatment can be used to inhibit undesired reactions (cracking, hydrogenolysis, dealkylation) and enhance selectivity to styrene. Pre-coking with benzene was the most effective pre-treatment, with styrene demonstrating similar efficacy. This is a result of the removal of hydroxyl groups due to the presence of significant coke deposits, and the associated change in chromium oxidation state to Cr(III), the active species for dehydrogenation. Pre-coking

with aromatic molecules led to the deposition of naphthenic coke structures which are beneficial for dehydrogenation since they result in the deactivation of acid sites and Cr-VI(O) sites. Conversely, coke formed from ethylene was found to be detrimental for dehydrogenation activity as shown by the decrease in styrene selectivity as compared to the fresh catalyst.

Acknowledgements

The authors express their appreciation to the support from the Ministry of Higher Education, Saudi Arabia, in establishment of the Center of Research Excellence in Petroleum Refining & Petrochemicals at King Fahd University of Petroleum & Minerals (KFUPM).

4. References

1 M. Guisnet and P. Magnoux, *Appl. Catal.*, 1989, **54**, 1–27.

2 E. G. Derouane, *Catalysis by Acids and Bases*, Elsevier, Amsterdam, 1985, vol. 20.

3 P. Marécot, A. Akhachane and J. Barbier, *Catal. Letters*, 1996, **36**, 37–39.

4 C. Hettige, K. R. R. Mahanama and D. P. Dissanayake, *Chemosphere*, 2001, **43**, 1070–1083.

5 W. W. Kaeding, C. Chu, L. B. Young, B. Weinstein and S. A. Buttery, *J. Catal.*, 1981, **67**, 159–174.

6 J. Houzvicka, R. Pestman and V. Ponec, *Catal. Letters*, 1995, **30**, 289–296.

7 D. Chen, H. P. Rebo, K. Moljord and A. Holmen, *Stud. Surf. Sci. Catal.*, 1997, **111**, 159–166.

8 J. McGregor, Z. Huang, E. P. J. Parrott, J. A. Zeitler, K. L. Nguyen, J. M. Rawson, A. Carley, T. W. Hansen, J.-P. Tessonnier, D. S. Su, D. Teschner, E. M. Vass, A. Knop-Gericke, R. Schlögl and L. F. Gladden, *J. Catal.*, 2010, **269**, 329–339.

9 S. J. Thomson and G. Webb, *J. Chem. Soc. Chem. Commun.*, 1976, 526.

10 I. M. Dahl and S. Kolboe, *Catal. Letters*, 1993, **20**, 329–336.

11 F. Bauer, W.-H. Chen, H. Ernst, S.-J. Huang, A. Freyer and S.-B. Liu, *Microporous Mesoporous Mater.*, 2004, **72**, 81–89.

12 M. Niwa, H. Ito, S. Kato, T. Hattori and Y. Murakami, *J. Chem. Soc. Chem. Commun.*, 1982, 819–820.

13 H. Begum, N. Katada and M. Niwa, *Microporous Mesoporous Mater.*, 2001, **46**, 13–21.

14 W. O. Haag, D. H. Olson and F. Gorra, *US Pat. No. 4 097 543*, 1982, assigned to Mobil Oil Corporation.

15 F. Gorra, L. L. Breckenridge, W. M. Guy and R. A. Sailor, *Oil Gas J.*, 1992, **90**, 60–67.

16 G. Yaluris, R. B. Larson, J. M. Kobe, M. R. González, K. B. Fogash and J. A. Dumesic, *J. Catal.*, 1996, **158**, 336–342.

17 J.-H. Kim, Y. Sugi, T. Matsuzaki, T. Hanaoka, Y. Kubota, X. Tu, M. Matsumoto, S. Nakata, A. Kato, G. Seo and C. Pak, *Appl. Catal. A Gen.*, 1995, **131**, 15–32.

18 R. Fiedorow, R. Frański, A. Krawczyk and S. Beszterda, *J. Phys. Chem. Solids*, 2004, **65**, 627–632.

19 J. McGregor and L. F. Gladden, *Appl. Catal. A Gen.*, 2008, **345**, 51–57.

20 S. Mandal, A. K. Das and S. Ghosh, *Ind. Eng. Chem. Res.*, 1993, **32**, 1018–1023.

21 C. K. Lee, L. F. Gladden and P. J. Barrie, *Appl. Catal. A Gen.*, 2004, **274**, 269–274.

22 C. Venkat, in *19th Dewitt Petrochemical Review*, 1994, pp. A1–A11.

23 C. D. Low, R. J. Lawson, P. J. Kuchar and G. L. Gray, *US Pat. No. 5 321 184*, 1994, assigned to UOP.

24 W. O. Haag and D. H. Olson, *US Pat. No. 4 117 026*, 1978, to Mobil Oil Corporation.

25 W. O. Haag, D. H. Olson and P. G. Rodewald, *US Pat. No. 4 508 836*, 1985, to Mobil Oil Corporation.

26 S. Laforge, D. Martin and M. Guisnet, *Microporous Mesoporous Mater.*, 2004, **67**, 235–244.

27 F. Bauer, W. H. Chen, E. Bilz, A. Freyer, V. Sauerland and S. B. Liu, *J. Catal.*, 2007, **251**, 258–270.

28 B. M. Weckhuysen and R. A. Schoonheydt, *Catal. Today*, 1999, **51**, 223–232.

29 S. De Rossi, M. P. Casaletto, G. Ferraris, A. Cimino and G. Minelli, *Appl. Catal., A Gen.*, 1998, **167**, 257–270.

30 M. Cherian, M. S. Rao, A. M. Hirt, I. E. Wachs and G. Deo, *J. Catal.*, 2002, **211**, 482–495.

31 P. C. Upadhya, K. L. Nguyen, Y. C. Shen, J. Obradovic, K. Fukushige, R. Griffiths, L. F. Gladden, A. G. Davies and E. H. Linfield, *Spectrosc. Lett.*, 2006, **39**, 215–224.

32 E. P. J. Parrott, J. A. Zeitler, J. McGregor, S.-P. Oei, H. E. Unalan, S.-C. Tan, W. I. Milne, J.-P. Tessonnier, R. Schlögl and L. F. Gladden, *J. Phys. Chem. C*, 2009, **113**, 10554–10559.

33 S. Gomez, L. McMillan, J. McGregor, J. A. Zeitler, N. Al-Yassir, S. Al-Khattaf and L. F. Gladden, *Cat. Sci. Tech.*, 2015.

34 O. Bayraktar and E. L. Kugler, *Appl. Catal. A Gen.*, 2002, **233**, 197–213.

35 F. Tuinstra and J. L. Koenig, *J. Chem. Phys.*, 1970, **53**, 1126–1130.

36 O. Beyssac, B. Goffe, J.-P. Petitet, E. Froigneux, M. Moreau and J.-N. Rouzaud, *Spectrochim. Acta, Part A*, 2003, **59A**, 2267–2276.

37 A. Sadezky, H. Muckenhuber, H. Grothe, R. Niessner and R. Pöschl, *Carbon N. Y.*, 2005, **43**, 1731–1742.

38 W. Shen, Z. Li and Y. Liu, *Recent Patents Chem. Eng.*, 2008, **1**, 27–40.

39 J. Coates, in *Encyclopedia of Analytical Chemistry*, ed. R. A. Meyers, John Wiley & Sons Ltd., Chichester, 2000, pp. 10815–10837.

40 Schroeder P A, in *Teaching Clay Science*, Steve Guggenheim and Audrey Rule, Clay Minerals Society Workshop Series, Aurora, 2002, vol. 11, pp. 181–202.

41 A. A. Davydov, in *Infrared Spectroscopy of Adsorbed Species on the Surface of Transition Metal Oxides*, ed. C. H. R. (Eds.), John Wiley & Sons, Inc., 1984, pp. 6–62.

42 R. B. Fahim, M. I. Zaki, N. E. Fouad, M. Abdel-Khali and N. Sheppard, *Appl. Catal. A Gen.*, 2004, **265**, 229–235.

43 T. J. Bandosz, in *Surface Chemistry of carbon materials*, eds. P. Serp and J. L. Figueiredo, John Wiley & Sons, Inc., New Jersey, NJ, USA, 2009, pp. 45–92.

44 S. M. K. Airaksinen, A. O. I. Krause, J. Sainio, J. Lahtinen, K.-J. Chao, M. O. Guerrero-Pérez and M. A. Bañares, *Phys. Chem. Chem. Phys.*, 2003, **5**, 4371–4377.

45 K. Ramasesha, L. De Marco, A. Mandal and A. Tokmakoff, *Nat. Chem.*, 2013, **5**, 935–940.

46 M. Muhler, J. Schütze, M. Wesemann, T. Rayment, A. Dent, R. Schlögl and G. Ertl, *J. Catal.*, 1990, **126**, 339–360.

47 O. F. Gorriz, V. Cortes Corberan and J. L. G. Fierro, *Ind. Eng. Chem. Res.*, 1992, **31**, 2670–2674.

48 F. Cavani, M. Koutyrev, F. Trifirò, A. Bartolini, D. Ghisletti, R. Iezzi, A. Santucci and G. Del Piero, *J. Catal.*, 1996, **158**, 236–250.

49 T. W. Lyons, D. Guironnet, M. Findlater and M. Brookhart, *J. Am. Chem. Soc.*, 2012, **134**, 15708–11.

50 A. Chakrabarti and I. E. Wachs, *Catal. Letters*, 2014, **145**, 985–994.

51 US Pat. 2920114 (1960).

52 US Pat. 5786431 (1998).

53 M. Frenklach, W. C. Gardiner, S. E. Stein, D. W. Clary and T. Yuan, *Combust. Sci. Technol.*, 1986, **50**, 79–115.

List of Figure captions

Fig. 1. Conversion of ethylbenzene (△) and selectivity to toluene (▲), benzene (■) and styrene (◆) after ethylbenzene dehydrogenation over CrO_x/Al_2O_3 at 600 °C [33].

Fig. 2. TPO of fresh CrO_x/Al_2O_3 after ethylbenzene dehydrogenation and after pre-coking with benzene, toluene, styrene and ethylene at 600 °C.

Fig. 3. TPD (helium flow rate =40 ml/min, 5 °C/min) of pre-coked CrO_x/Al_2O_3 with a) toluene, b) benzene, c) styrene and d) ethylene.

Fig. 4. Raman spectra of fresh CrO_x/Al_2O_3 after ethylbenzene dehydrogenation (---) and after pre-coking (–), with a) toluene, b) benzene, c) styrene and d) ethylene.

Fig. 5. DRIFTS difference spectra of CrO_x/Al_2O_3 after pre-coking with a) toluene, b) benzene, c) styrene and d) ethylene at 600 °C, obtained by subtracting the spectrum of fresh CrO_x/Al_2O_3 from those of the pre-coked catalysts, such that the resulting absorptions are attributed to the coke deposits present on the catalyst surface.

Fig. 6. Diffuse reflectance infrared Fourier transform spectroscopy of fresh CrO_x/Al_2O_3 after ethylbenzene dehydrogenation at 600 °C.

Fig. 7. FTIR spectra of a) 1-methyl naphthalene and b) *p*-xylene (NIST Chemistry Web Book; http:/webbook.nist.gov).

Fig. 8. Selectivity to toluene (▲), benzene (■) and styrene (◆) for ethylbenzene dehydrogenation (600 °C, 6 h time-on-stream) over CrO_x/Al_2O_3 pre-coked with a) ethylene, b) toluene, c) benzene and d) styrene. The inset plots show the conversion of ethylbenzene (△) *versus* time-on-stream.

Fig. 9. Selectivity to styrene over pre-coked CrO_x/Al_2O_3 *versus* a) C/H ratio, b) oxidation temperature, and c) THz absorption coefficient at 1 THz and d) % reduction of OH band (3520 cm^{-1}) from DRIFTS.

Fig. 10. Temperature-programmed oxidation of pre-coked catalysts after ethylbenzene dehydrogenation at 600 °C (40 ml/min, 5% O_2/He, 5 °C/min).

Fig. 11. Fig. 7. THz spectra of CrO_x/Al_2O_3 after (a) ethylbenzene dehydrogenation at 600 °C, after pre-coking at 600 ºC with (b) toluene (c) ethylene, (d) styrene, (e) benzene; and ethylbenzene dehydrogenation over pre-coked CrO_x/Al_2O_3 with f) benzene, g) toluene, (h) styrene and (i) ethylene.

Tables

Table 1. Elemental microanalysis showing the wt. % carbon and hydrogen and C/H mass ratio after pre-coking with benzene, toluene, styrene and ethylene over CrO_x/Al_2O_3 catalysts at 600 °C for 6 h time-on-stream and fresh CrO_x/Al_2O_3 after ethylbenzene dehydrogenation at 600 °C for 6 h time-on-stream.

CrO_x/Al_2O_3 pre-coked with:	**%C (wt. %)**	**%H (wt. %)**	**C/H mass ratio**	**$\%C_{coke}$**
benzene	11.1 ± 0.1	0.8 ± 0.1	13.9 ± 0.9	93.3 ± 0.4
toluene	8.9 ± 0.1	0.9 ± 0.1	9.9 ± 0.2	90.8 ± 0.2
styrene	10.7 ± 0.1	0.7 ± 0.1	15.2 ± 0.9	93.9 ± 0.3
ethylene	2.7 ± 0.1	0.6 ± 0.1	4.5 ± 0.2	81.8 ± 0.7
CrO_x/Al_2O_3 after EB dehydrogenation	6.3 ± 0.2	0.6 ± 0.1	10.5 ± 0.9	91.3 ± 0.6

Table 2. Classification of coke structures according to their C/H mass ratio and $\%C_{coke}$. The square and round brackets show closed an open intervals respectively.

Coke structure	C/H mass ratio range	$\%C_{coke}$ range
linear alkanes (C_nH_{2n+2})	[3, 6)	[75, 85.7)
linear alkenes with 1 double bond (C_nH_{2n})	6	85.7
linear alkenes with *n* double bonds	(6, 4n]	[85.7, 100)
cycloalkanes ($(CH_2)_n$)	6	85.7
cycloalkenes (C_nH_{2n-2})	(6, 8]	(85.7, 88.9]
benzene (C_6H_6)	12	92.3
alkylaromatics	(6, 12)	(85.7, 92.3)
linear polyaromatics with 6 membered-rings	[15, 24)	[93.8, 96)
non-linear polyaromatics with 6 membered-rings	[16.8, 24)	[94.4, 96)
polyaromatics with *n* membered-rings (mixture of 4, 5, 6…n membered-rings)	(12, 24)	(92.3, 96)

Table 3. Comparison of catalytic performance of fresh and pre-coked CrO_x/Al_2O_3 for ethylbenzene dehydrogenation at 600 °C. The average error in conversion and selectivity values is ~5 % of the stated value.

Conversion and selectivity of ethylbenzene dehydrogenation over:					
	fresh CrO_x/Al_2O_3	**ethylene pre-coked CrO_x/Al_2O_3**	**toluene pre-coked CrO_x/Al_2O_3**	**benzene pre-coked CrO_x/Al_2O_3**	**styrene pre-coked CrO_x/Al_2O_3**
% Conversion	97	98	90	87	94
% Selectivity					
toluene	1.3	0.5	0.7	0.9	0.8
benzene	2.9	0.4	0.8	1.0	0.4
styrene	15.1	11.4	24.4	31.0	29.1
methane	0.3	0.2	0.3	0.2	0.3
ethylene	0.3	0.2	0.3	0.2	0.3
coke	80.1	87.3	73.5	66.7	69.1
Time to reach steady state (min)	185	205	245	145	165
Induction time (min)	145	25	0	0	0

Table 4. Number of acid sites and acidity distribution of CrO_x/Al_2O_3. a) Fresh, b) after 3 h of ethylbenzene dehydrogenation (cracking period), c) after 6 h of ethylbenzene dehydrogenation and d) after pre-coking with benzene.

Sample	Acidity distribution	μmol NH_3/g
Fresh CrO_x/Al_2O_3	low strength	202 ± 7
	medium strength	191 ± 6
	high strength	101 ± 4
	total	494 ± 17
CrO_x/Al_2O_3 after cracking period (3 h)	low strength	167 ± 6
	medium strength	207 ± 7
	high strength	70 ± 4
	total	444 ± 17
CrO_x/Al_2O_3 after dehydrogenation period (6 h)	low strength	103 ± 5
	medium strength	121 ± 2
	high strength	40 ± 1
	total	264 ± 8
CrO_x/Al_2O_3 pre-coked with benzene	low strength	86 ± 3
	medium strength	115 ± 4
	high strength	42 ± 1
	total	243 ± 8

Table 5. Cr(III)/Cr(VI) ratios for fresh CrO_x/Al_2O_3, after ethylbenzene dehydrogenation for 1, 3 and 6 h time-on-stream and after pre-coking with benzene.

Sample	Cr(III)/Cr(VI)
Fresh CrO_x/Al_2O_3	0.3 ± 0.02
CrO_x/Al_2O_3 - 600 °C - 1 h time-on-stream	1.1 ± 0.07
CrO_x/Al_2O_3 - 600 °C - 3 h time-on-stream	2.2 ± 0.13
CrO_x/Al_2O_3 - 600 °C - 6 h time-on-stream	2.0 ± 0.13
CrO_x/Al_2O_3 pre-coked with benzene	1.2 ± 0.06

Table 6. Elemental analysis of pre-coked and reacted CrO_x/Al_2O_3 after ethylbenzene dehydrogenation at 600 °C.

ethylbenzene dehydrogenation over:	%C (wt. %)	%H (wt. %)	C/H mass ratio	$\%C_{coke}$
Fresh CrO_x/Al_2O_3 - 6 h, 600 °C	6.3 ± 0.2	0.6 ± 0.1	10.5 ± 0.9	91.3 ± 0.7
CrO_x/Al_2O_3 pre-coked with benzene - 6 h, 600 °C	13.5 ± 0.1	0.9 ± 0.1	15.0 ± 0.8	93.8 ± 0.3
CrO_x/Al_2O_3 pre-coked with toluene - 6 h, 600 °C	15.4 ± 0.1	0.9 ± 0.1	17.1 ± 0.2	94.5 ± 0.1
CrO_x/Al_2O_3 pre-coked with styrene - 6 h, 600 °C	21.4 ± 0.1	0.9 ± 0.1	23.8 ± 1.2	95.9 ± 0.3
CrO_x/Al_2O_3 pre-coked with ethylene - 6 h, 600 °C	14.9 ± 0.2	0.5 ± 0.1	29.8 ± 2.0	96.8 ± 0.2

Table 7. Position of the Raman bands, D1/G and D1/D3 ratios of pre-coked catalysts after ethylbenzene dehydrogenation at 600 °C for 6 h time-on-stream.

		ethylbenzene dehydrogenation over CrO_x/Al_2O_3 pre-coked with:			
		benzene	**toluene**	**styrene**	**ethylene**
D4	position (cm^{-1})	1208	1223	1223	1205
	FWHM (cm^{-1})	58	97	98	76
D1	position (cm^{-1})	1309	1328	1329	1318
	FWHM (cm^{-1})	148	159	153	158
D3	position (cm^{-1})	1486	1475	1466	1501
	FWHM (cm^{-1})	167	172	167	170
G	position (cm^{-1})	1598	1595	1592	1593
	FWHM (cm^{-1})	56	72	76	66
Intensity ratios					
D1/G		3.0 ± 0.1	2.2 ± 0.1	2.0 ± 0.1	1.9 ± 0.1
D1/D3		3.7 ± 0.2	2.3 ± 0.1	2.8 ± 0.1	4.9 ± 0.2

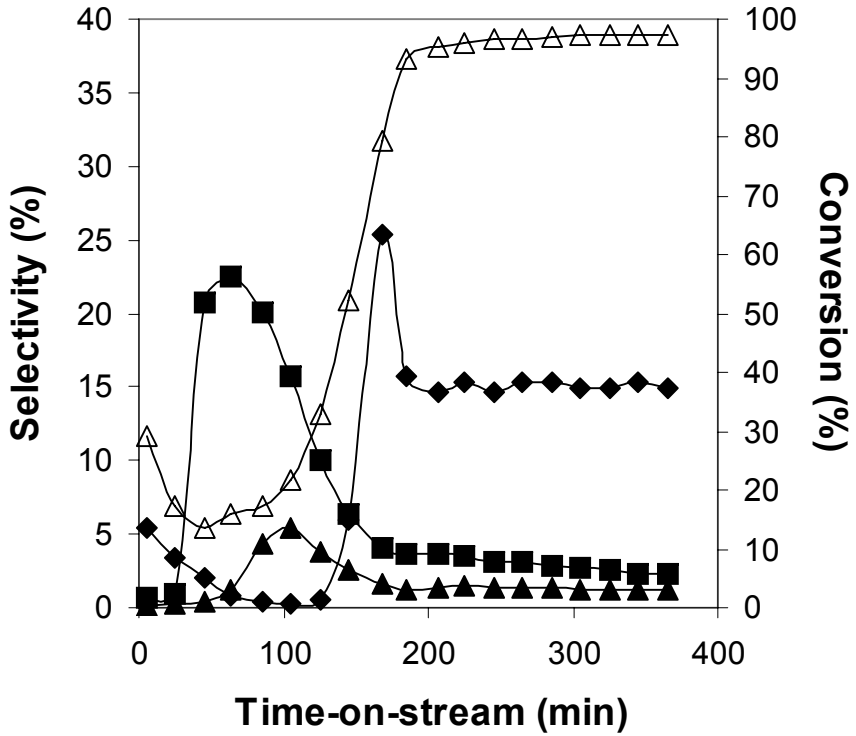

Fig. 1. Conversion of ethylbenzene (△) and selectivity to toluene (▲), benzene (■) and styrene (◆) after ethylbenzene dehydrogenation over CrO_x/Al_2O_3 at 600 °C [31].

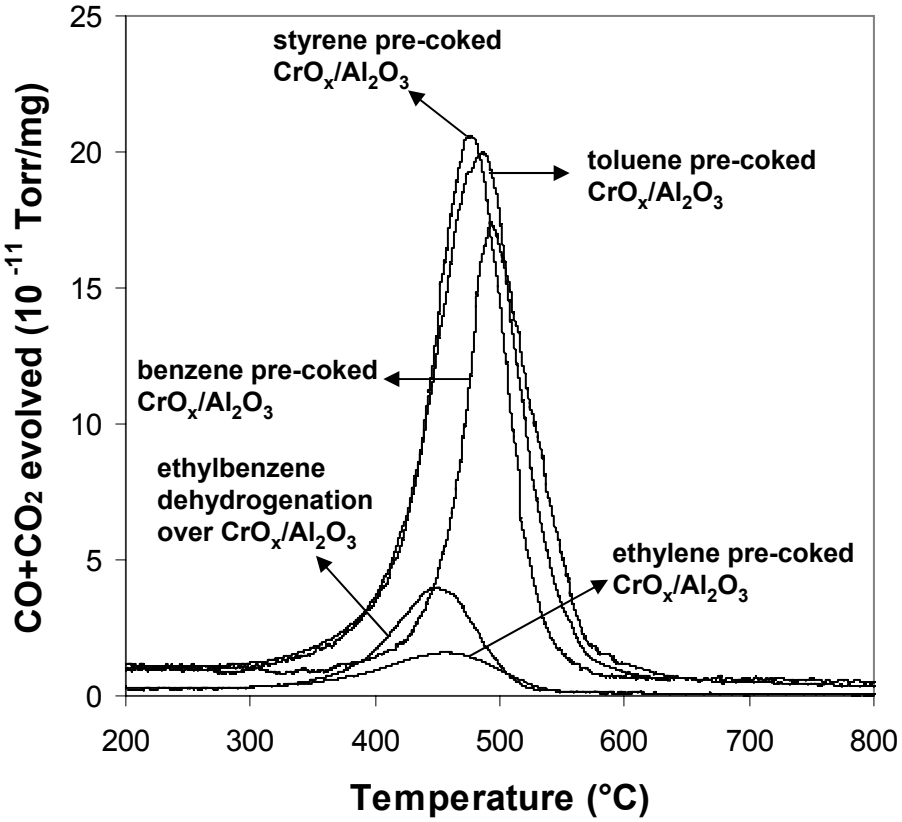

Fig. 2. TPO of fresh CrO_x/Al_2O_3 after ethylbenzene dehydrogenation and after pre-coking with benzene, toluene, styrene and ethylene at 600 °C.

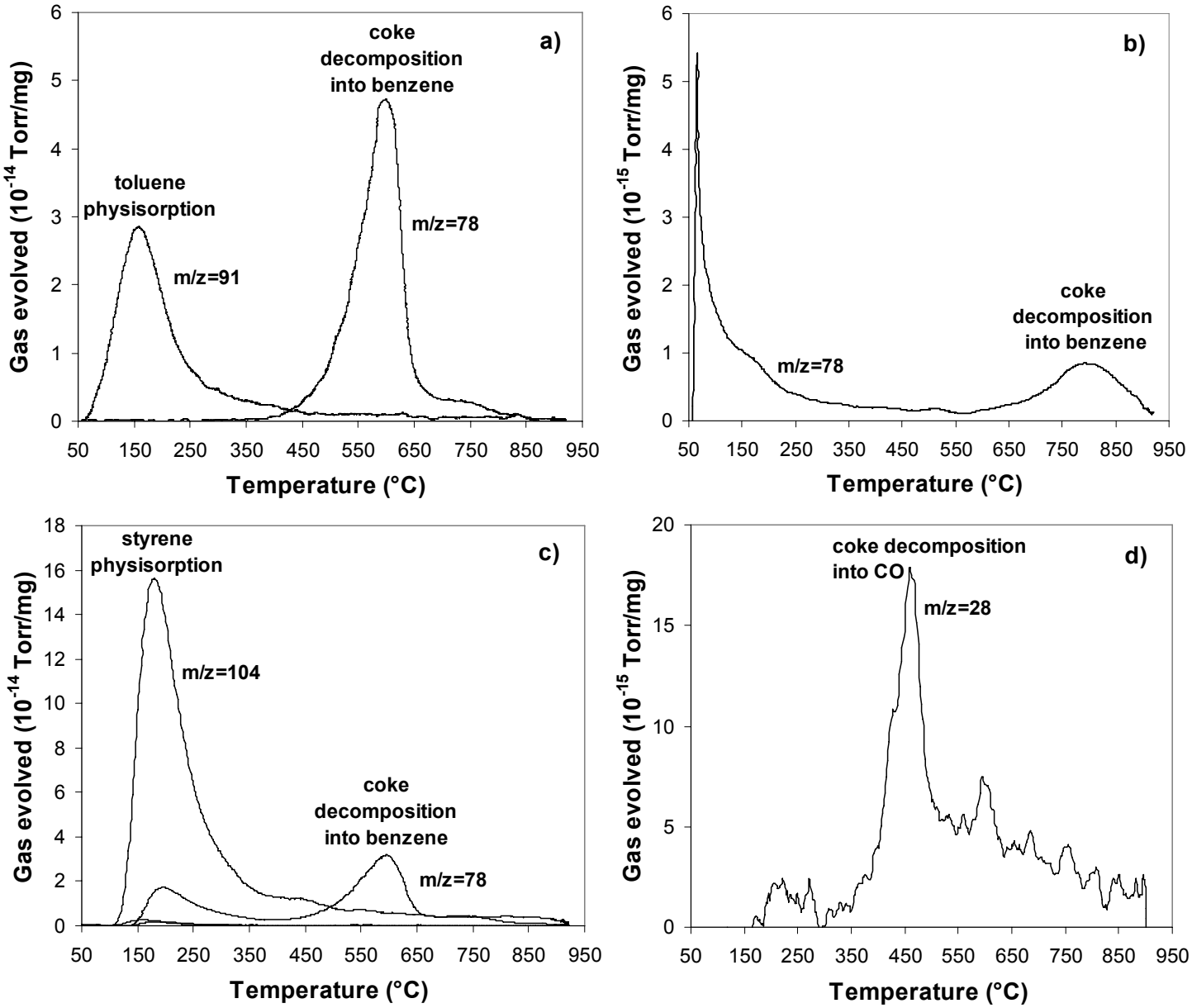

Fig. 3. TPD (helium flow rate = 40 ml/min, 5 °C/min) of pre-coked CrO_x/Al_2O_3 with a) toluene, b) benzene, c) styrene and d) ethylene.

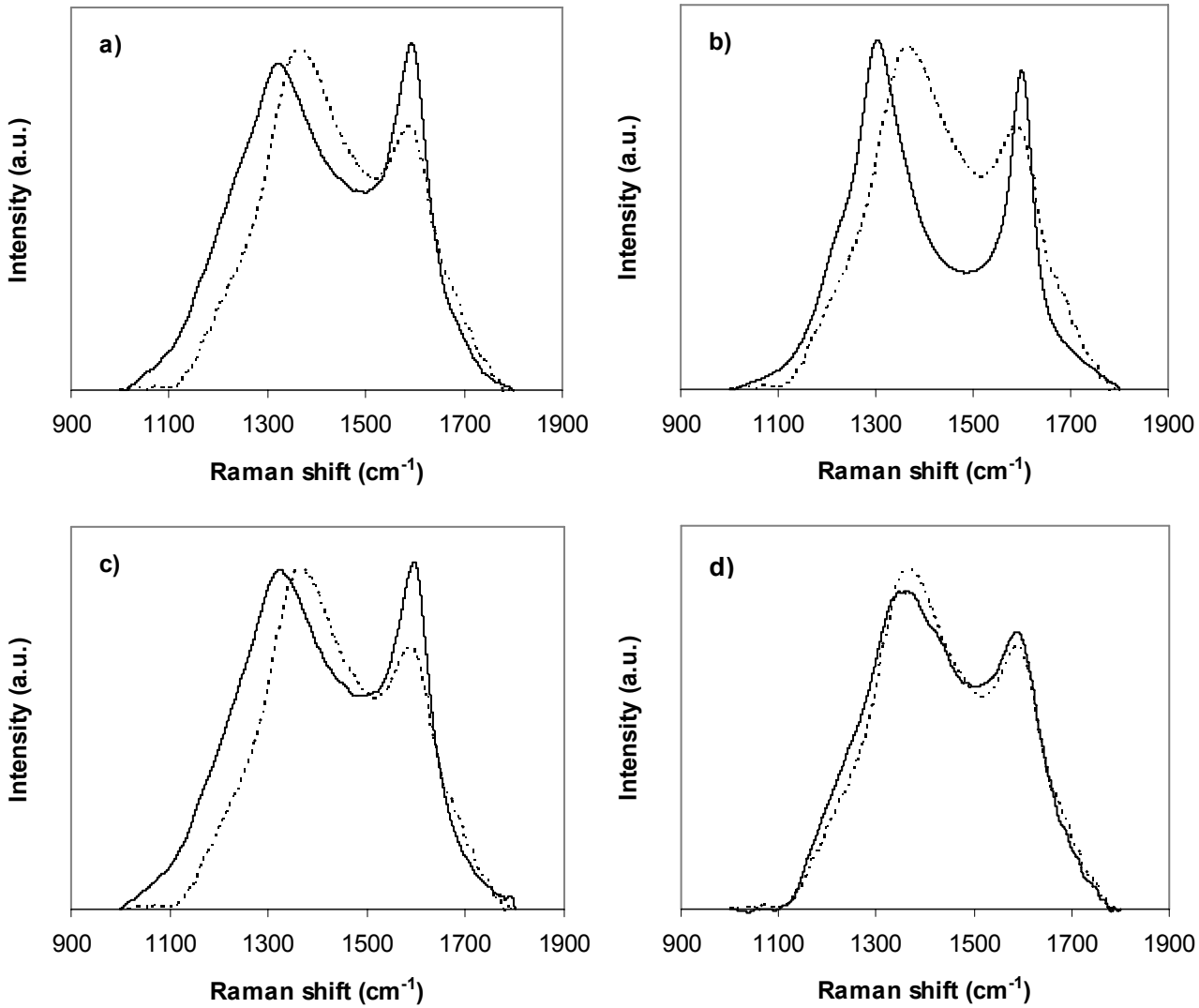

Fig. 4. Raman spectra of fresh CrO_x/Al_2O_3 after ethylbenzene dehydrogenation (--) and after pre-coking (–), with a) toluene, b) benzene, c) styrene and d) ethylene.

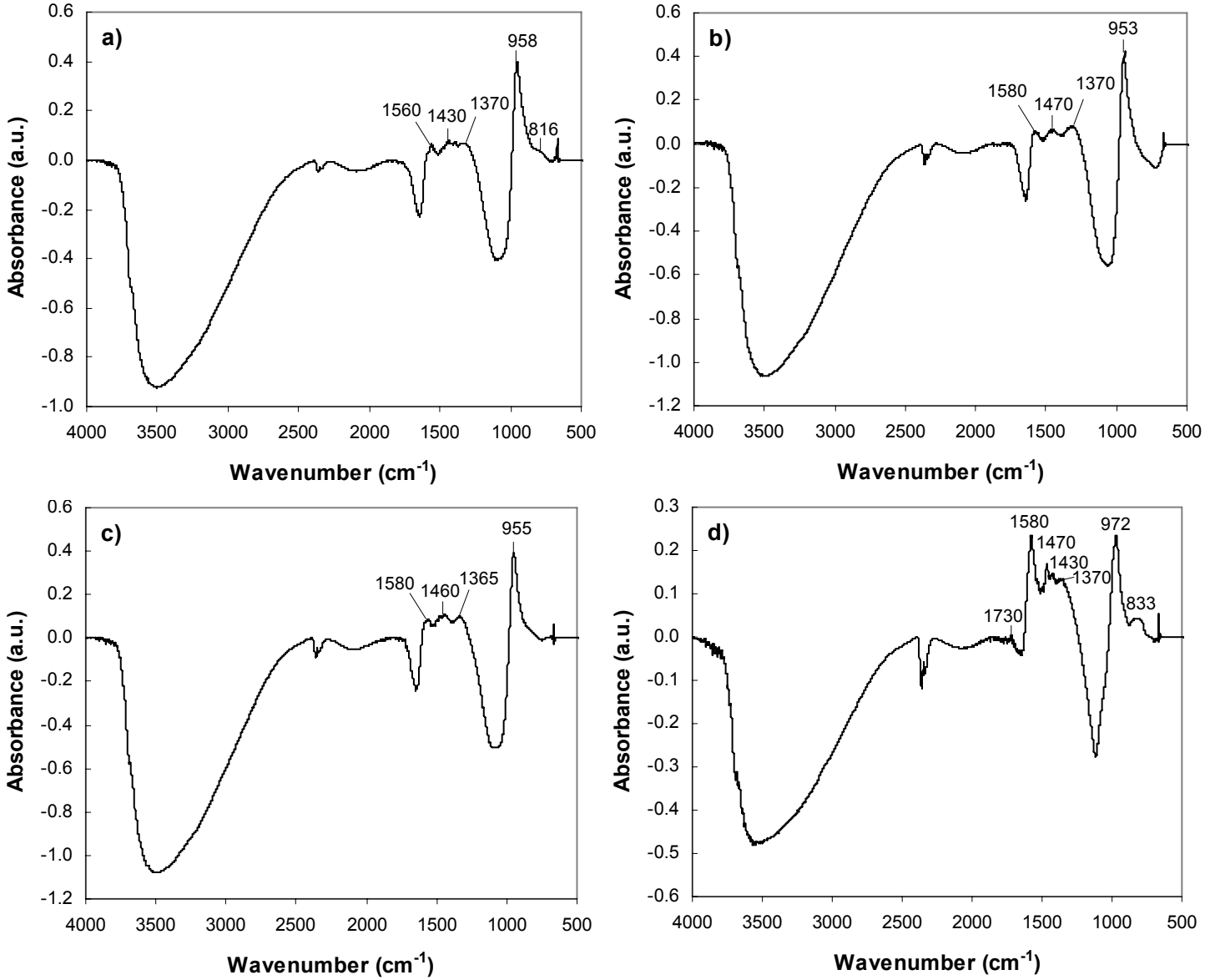

Fig. 5. DRIFTS difference spectra of CrO_x/Al_2O_3 after pre-coking with a) toluene, b) benzene, c) styrene and d) ethylene at 600 °C, obtained by subtracting the spectrum of fresh CrO_x/Al_2O_3 from those of the pre-coked catalysts, such that the resulting absorptions are attributed to the coke deposits present on the catalyst surface.

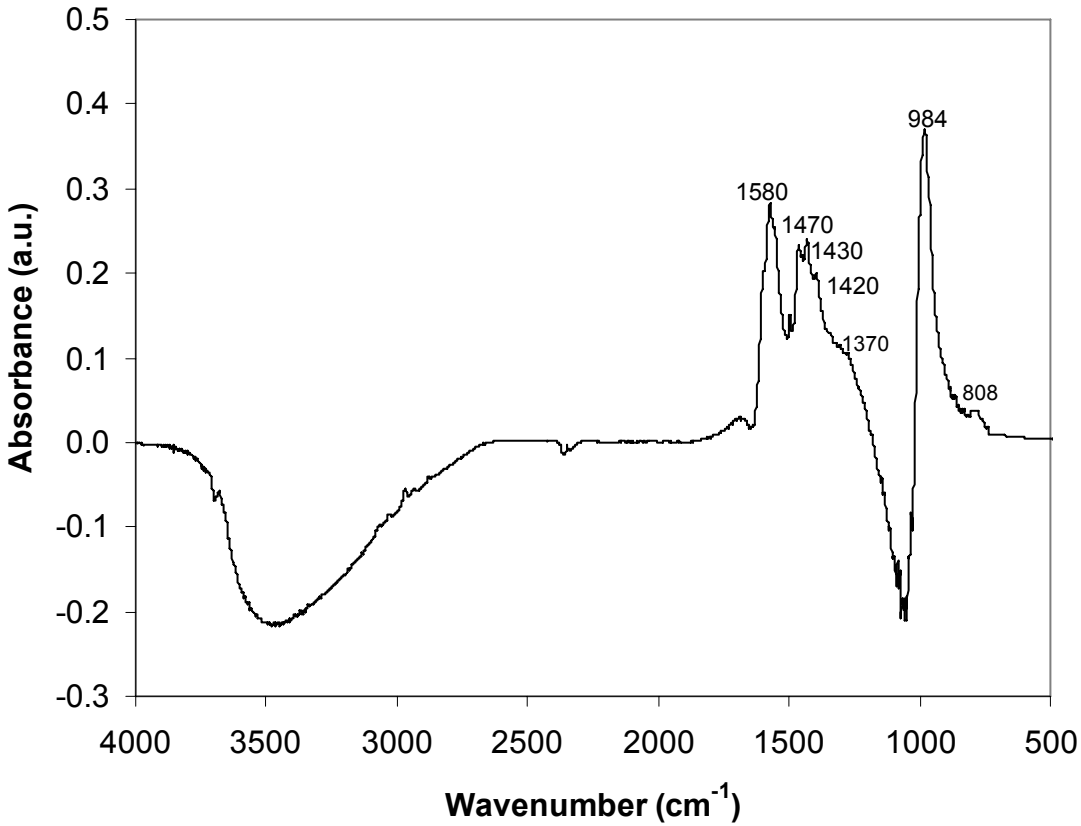

Fig. 6. Diffuse reflectance infrared Fourier transform spectroscopy of fresh CrO_x/Al_2O_3 after ethylbenzene dehydrogenation at 600 °C.

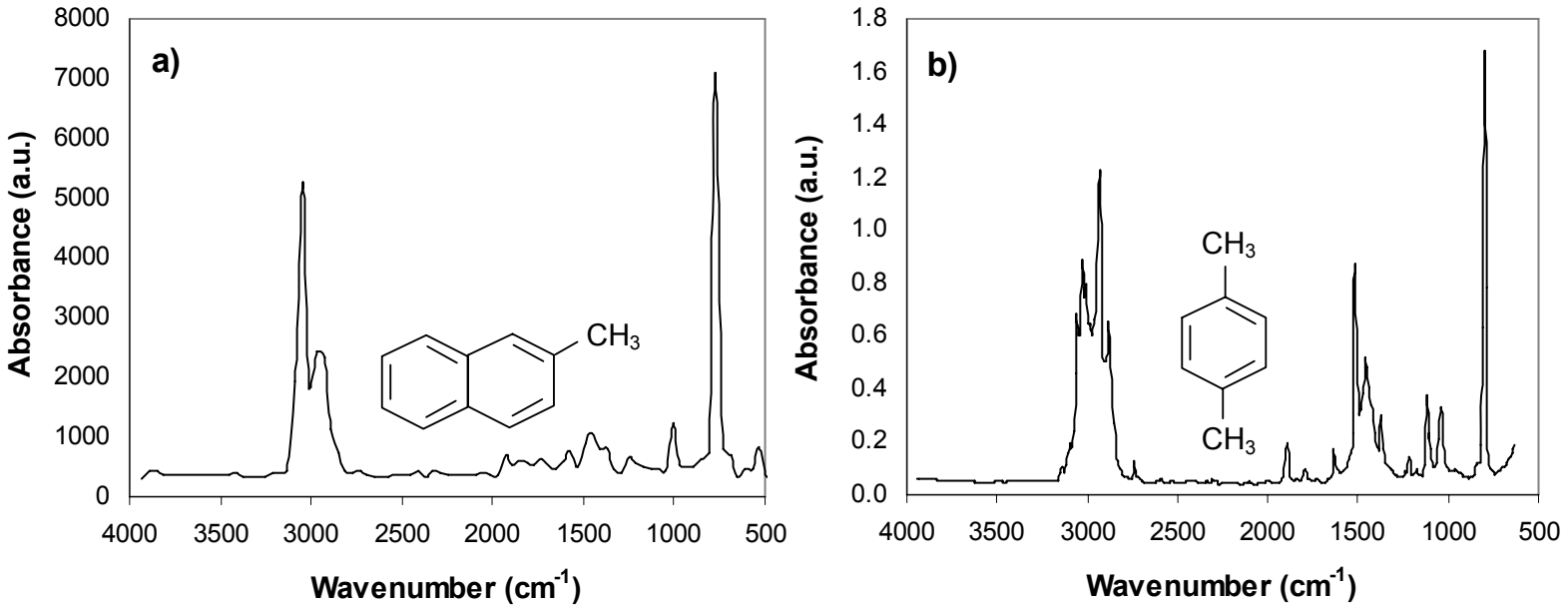

Fig. 7. FTIR spectra of a) 1-methyl naphthalene and b) *p*-xylene (NIST Chemistry Web Book; http:/webbook.nist.gov)

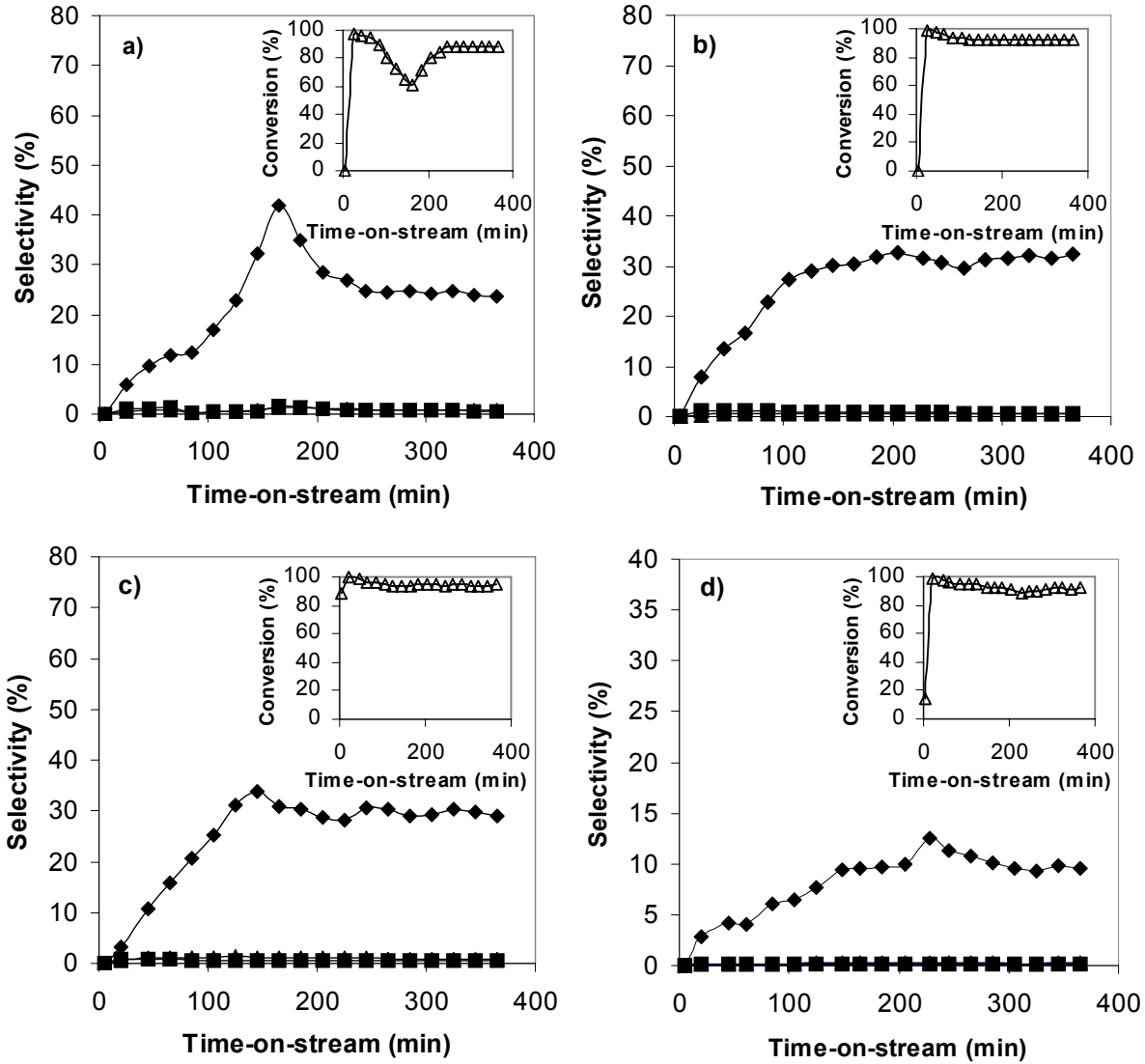

Fig. 8. Selectivity to toluene (▲), benzene (■) and styrene (◆) for ethylbenzene dehydrogenation (600 °C, 6 h time-on-stream) over CrO_x/Al_2O_3 precoked with a) toluene, b) benzene, c) styrene and d) ethylene. The inset plots show the conversion of ethylbenzene (△) *versus* time-on-stream.

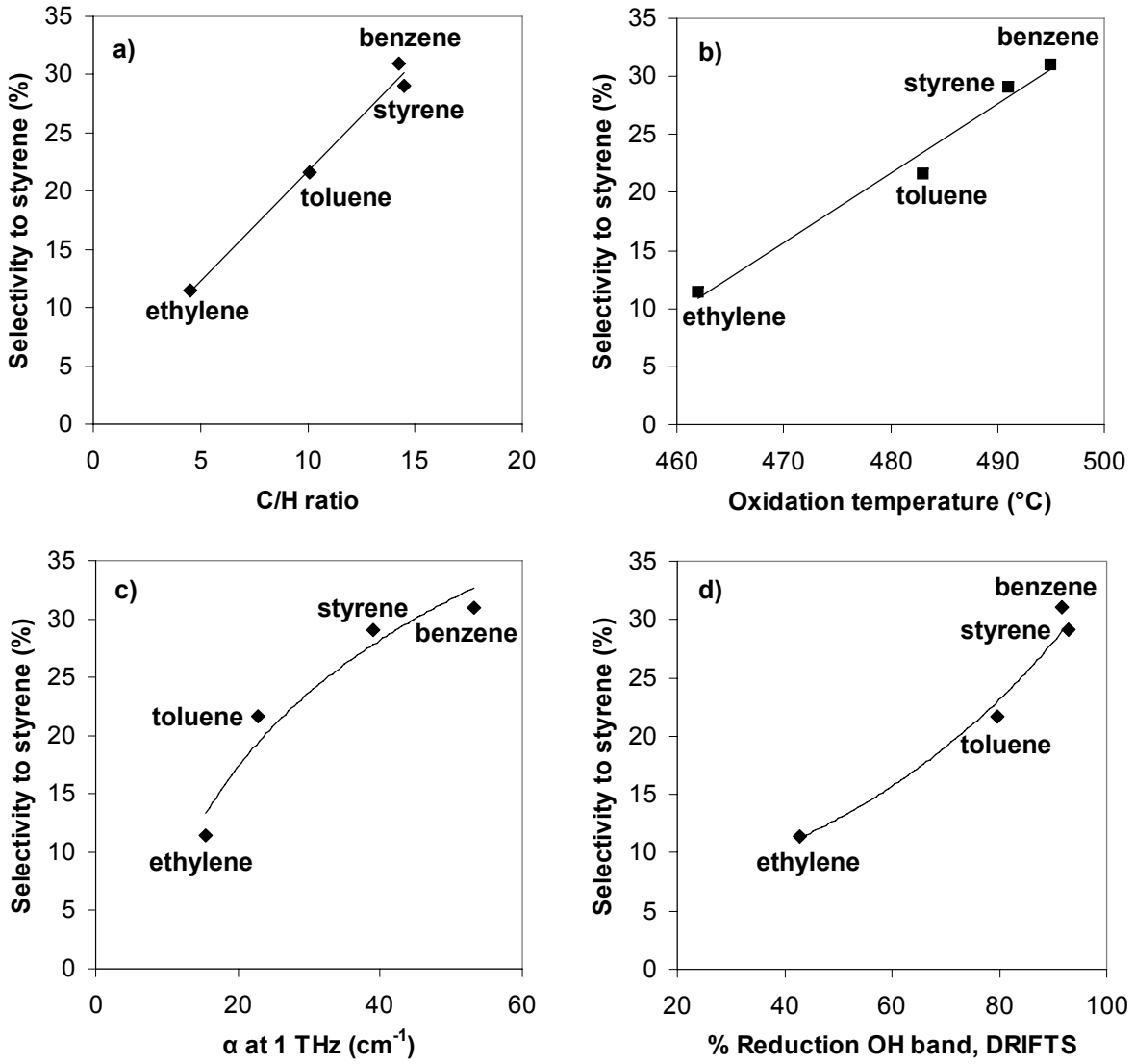

Fig. 9. Selectivity to styrene over pre-coked CrO_x/Al_2O_3 *versus* a) C/H ratio, b) oxidation temperature, c) THz absorption coefficient (α) at 1 THz and d) % reduction of OH band (3520 cm^{-1}) from DRIFTS.

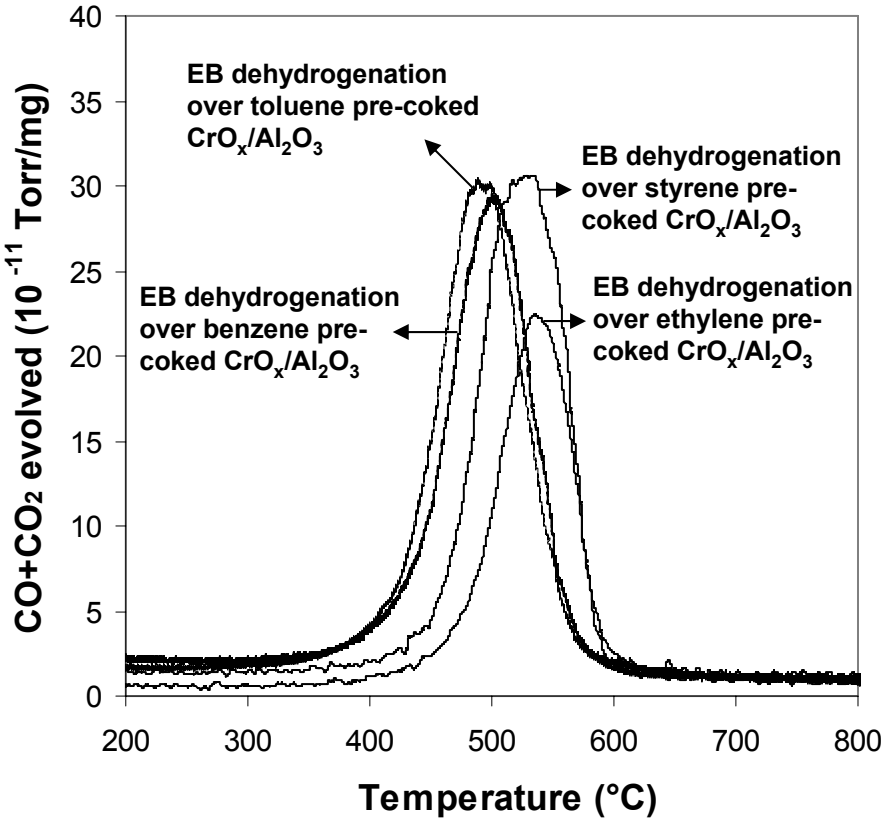

Fig. 10. Temperature-programmed oxidation of pre-coked catalysts after ethylbenzene dehydrogenation at 600 °C (40 ml/min, 5% O_2/He, 5 °C/min).

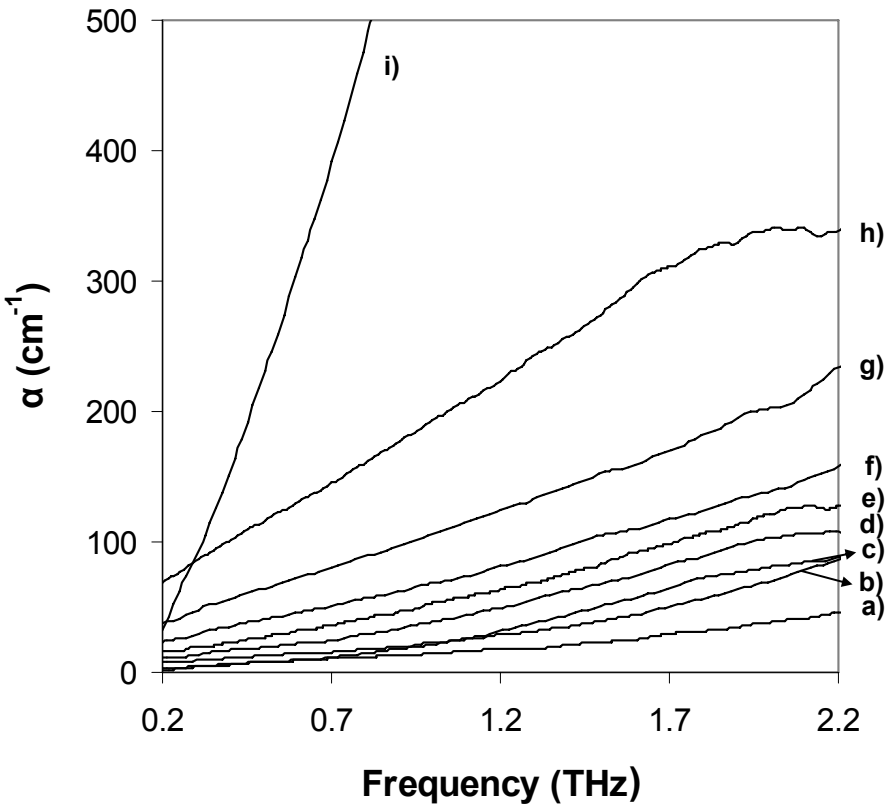

Fig. 11. THz spectra of CrO_x/Al_2O_3 after (a) ethylbenzene dehydrogenation at 600 °C, after pre-coking at 600 ºC with (b) toluene (c) ethylene, (d) styrene, (e) benzene; and ethylbenzene dehydrogenation over pre-coked CrO_x/Al_2O_3 with f) benzene, g) toluene, (h) styrene and (i) ethylene.

The origin and role of coke in ethylbenzene dehydrogenation over CrO_x/Al_2O_3 has been investigated through pre-coking studies. Ethylene is main coke precursor, leading to catalyst deactivation; however coke from aromatic species is beneficial for styrene production.